Accepted Manuscript

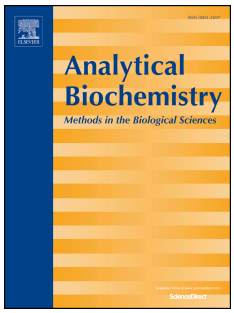

Aptamer-based electrochemical biosensor by using Au-Pt nanoparticles, carbon nanotubes and acriflavine platform

Zeinab Sahraei Beiranvand, Amir Reza Abbasi, Sara Dehdashtian, Ziba Karimi, Azadeh Azadbakht

PII: S0003-2697(16)30313-X

DOI: 10.1016/j.ab.2016.10.001

Reference: YABIO 12519

To appear in: *Analytical Biochemistry*

Received Date: 29 June 2016

Revised Date: 28 September 2016

Accepted Date: 2 October 2016

Please cite this article as: Z.S. Beiranvand, A.R. Abbasi, S. Dehdashtian, Z. Karimi, A. Azadbakht, Aptamer-based electrochemical biosensor by using Au-Pt nanoparticles, carbon nanotubes and acriflavine platform, *Analytical Biochemistry* (2016), doi: 10.1016/j.ab.2016.10.001.

Aptamer-based electrochemical biosensor by using Au-Pt nanoparticles, carbon nanotubes and acriflavine platform

Zeinab Sahraei Beiranvand[a], Amir Reza Abbasi[a], Sara Dehdashtian[b], Ziba Karimi[a], Azadeh Azadbakht[a*]

[a]*Department of Chemistry, Khorramabad Branch, Islamic Azad University , Khorramabad, Iran.*

[b]*Department of Chemistry, Islamic Azad University, Omidieh Branch, Omidieh, Iran.*

Abstract

Herein, an ultrasensitive electrochemical aptasensor for quantitative detection of bisphenol A (BPA) was fabricated based on a novel signal amplification strategy. This aptasensor was developed by electrodeposition of gold-platinum nanoparticles (Au-PtNPs) on glassy carbon (GC) electrode modified with acid-oxidized carbon nanotubes (CNTs-COOH). In this protocol, acriflavine (ACF) was covalently immobilized at the surface of glassy carbon electrode modified with Au-PtNPs/CNTs-COOH nanocomposite. Attachment of BPA-aptamer at the surface of modified electrode was performed through the formation of phosphoramidate bonds between the amino group of ACF and phosphate group of the aptamer at 5'end. By interaction of BPA with the aptamer, the conformational of aptamer was changed which lead to retarding the interfacial electron transfer of ACF as a probe. Sensitive quantitative detection of BPA was carried out by monitoring the decrease of differential pulse voltammetric (DPV) responses of ACF peak current with increasing the BPA concentration. The resultant aptasensor exhibited good specificity, stability and reproducibility, indicating that the present strategy was promising for broad potential application.

Keywords: Aptasensor, Gold–platinum nanoparticles, Bisphenol A, Acriflavine.

*Corresponding author: A. Azadbakht, Tel: +98 6633120399
E-mail:Azadbakht.a@gmail.com

1. Introduction

Bisphenol A (BPA), as an important industrial chemical is widely used for the manufacture of polycarbonate plastics, epoxy resins, dental sealants, flame retardants, and food packaging. These kinds of materials are utilized as inner coating of food-storage or packaging materials, such as feeding bottles, food cans, water bottles, and tableware [1-3]. The global demand for BPA increased from 3.2 million tons in 2003 to 5.5 million tons in 2011 [4, 5]. When these materials expose to heat, the unstable and lipophilic compound BPA can migrate into drinking water and food by leaching from food storage and packaging materials, or release into environment through wastewater discharged from plastic-producing industry; thus, humans may routinely ingest trace amounts of BPA [6]. Extensive studies have indicated that BPA is an endocrine-disrupting chemical, which interfere with thyroid function, central nervous system, endocrine pancreas, immune system, reproduction system and hormonal activities in the growth, development and reproductive processes of aquatic animals [7]. Numerous types of cancers, cardiovascular disease, and diabetes are associated with the intake of BPA [8]. Therefore, development of specific, reliable, sensitive, and accurate method for determination of trace amount of BPA has attracted particular attention for public health and environmental security.

Various conventional analytical technologies have been developed for BPA determination such as liquid chromatography-mass spectrometry [9], liquid chromatography-tandem mass spectrometry [10], gas chromatography-mass spectrometry [9, 11], liquid chromatography-coulometric detection [12], liquid chromatography-fluorescence detection [13, 14], and liquid chromatography-UV detection [15]. All these techniques are restricted with extensive extraction, costly instruments, complicated and time-consuming sample preparation, skillful and experienced technician, and cleanup step.

Also, enzyme-linked immunosorbent assay has been employed for BPA detection with the advantages of high sensitivity, favorable selectivity, and possible analysis of complex matrices without extensive pretreatment [16]. Immunoassay-based methods are strongly dependent on the quality of the prepared antibody, which has been challenging due to the instability of the antibody and nonspecific binding to BPA analogs [17]. Hence, exploring a more efficient and selective technique for BPA detection is definitely necessary; consequently, colorimetric, optical and electrochemical sensors have been designed for BPA detection by employing aptamers as the molecular recognition elements [18-23].

Aptamers are nucleic acid ligands that can specifically recognize their targets. They isolate from a synthetic nucleic acid pool by Systematic Evolution of Ligands by EXponential enrichment (SELEX) and can specifically bind to a variety of target molecules

such as protein, small molecules, amino acids and even cells [24-29]. They are being an alternative to antibodies owning to the superior advantages over antibodies including temperature stability, easy artificial synthesis, specificity, low cost, and reusability. There is a growing interest for usage of aptamer in biorecognition area. Thus, fabrications of optic [30], fluorimetry [31], and electrochemical [32] aptasensors have received a significant attention.

How to convert the binding events between aptamer and target into a detectable electrochemical signal is the crucial point in the construction of electrochemical aptasensors. Generally, additional electroactive tags such as ferrocene derivatives, methylene blue, and ruthenium complexes [33-35], etc. have been employed to label aptamer to have the measurable signal. But labeling aptamer is a complicated and time-consuming process, even which might affect the affinity of aptamer toward target. Besides, electroactive compounds such as $[Fe(CN)_6]^{3-/\ 4-}$ can also be directly added into electrochemical cell to produce a measurable signal. Adding the redox probe directly in the test solution is usually prone to false-positive results produced by the limitations, including initial sensing interface contamination and additional incubations in the $[Fe(CN)_6]^{3-/\ 4-}$ between each measurements for a long time [36].

In the current paper, in order to overcome effectively these disadvantages of labeling aptamer or adding additional probe into test system, the acriflavine (ACF) as a redox probe was selected and in situ designed on the electrode surface due to its outstanding properties such as significant stability and good peak shape. CNTs-COOH decorated with gold–platinum nanoparticles (Au-PtNPs) was used as an effective immobilization matrix for covalent immobilization of ACF. Attachment of BPA-aptamer at the surface of modified electrode was performed through the formation of phosphoramidate bonds between the amino group of ACF and phosphate group of the aptamer at 5'end. Sensitive quantitative detection of BPA was carried out by monitoring the differences of the DPV response of the modified electrode before and after adding different concentration of BPA. The interaction of BPA with the aptamer caused the aptamer to be folded and the formation of BPA-aptamer complexes at the sensing interface hindered the interfacial electron transfer of the probe, resulting in the decrease of the electrochemical signal. Under the optimum conditions the prepared aptasensor had a wide linear response range, which proved that this method can be considered as an efficient method for constructing BPA electrochemical aptasensor with highly sensitivity and specificity.

2. Experimental

2.1. Chemicals

Multiwall carbon nanotubes with 95% purity, 10-20 nm diameters, and 1μm length were obtained from Nanolab (Brighton, MA). Potassium ferricyanide ($K_3Fe(CN)_6$), potassium ferrocyanide ($K_4Fe(CN)_6$), hydrogen tetrachloroaurate ($HAuCl_4.4H_2O$), hexachloroplatinate (IV) hydrate (H_2PtCl_6-$5H_2O$), nitric acid, ethanol, dimethyl sulfoxide (DMSO), and potassium chloride were obtained from Merck (Germany) and Fluka. N-hydroxysuccinimide (NHS), acriflavine, 1-ethyl-3-(3-dimethylaminopropyl) carbodiimide hydrochloride (EDC) and bisphenol A were purchased from Sigma and used as received without further purification. The BPA-aptamer with the sequence of 5'-CCG GTG GGT GGT CAG GTG GGA TAG CGT TCC GCG TAT GGC CCA GCG CAT CAC GGG TTC GCA CCA-3' was adopted according to the reported study [37]. All other chemicals were of analytical reagent grade and used without further purification. Phosphate buffered solution (PBS) was served as working buffer throughout the experiment, containing 0.1 M Na_2HPO_4, 0.1 M KH_2PO_4 and 0.1 M KCl. All experiments were performed at ambient temperature of 25 ±1◦C. Cyclic voltammetry (CV), electrochemical impedance spectroscopy (EIS), and differential pulse voltammetry (DPV) were recorded to study the fabrication of modified electrode. The EIS measurement was performed in the presence of 5.0 mM $K_3[Fe(CN)_6]/K_4[Fe(CN)_6]$ (1:1) and 0.1M PBS (pH=7.4). DPV was recorded with modulation amplitude of 0.05V, a pulse width of 0.05 s, and sample width of 0.0167s.

2.2. Apparatus

All electrochemical measurements were performed via using a μAutolab III potentiostat/galvanostat (Eco Chemie, The Switzerland). The experimental conditions were controlled with NOVA 1.8 and Frequency Response Analyzer (FRA) software. A conventional three electrode cell was employed with an Ag/AgCl electrode (KCl 3 M) as the reference electrode, a Pt wire as counter electrode and a modified glassy carbon (GC) electrode as working electrode. The cell was a one compartment cell with an internal volume of 10 ml. The pH was measured with a JENWAY pH meter (model 3345). The size and morphology of materials were investigated by taking scanning electron microscopy (SEM), energy-dispersive X-ray (EDS) spectroscopy and wavelength-dispersive X-ray (WDX) (X-30 Philips, Philip's Company, Netherlands).

2.3. Electrode treatment and aptamer immobilization

Prior to the modification, the GC electrode was polished with 0.3 and 0.05 μm

alumina slurry on a polishing cloth, followed by successive sonication in 1: 20 (v/v) nitric acid and ethanol to obtain a mirror-like surface. Then the GC electrode was cleaned in doubly distilled water in order to remove absorbed particles. After being dried in air, 10 µL of DMSO/CNTs-COOH solution (0.4 mg mL^{-1}) was cast at the surface of GC electrode to form a CNTs-COOH film at electrode surface. In order to prepare metal nanostructure film on the surface of electrode, electrodeposition is often used [38, 39] as an easy and controllable method which allows electrodeposited film tightly attaches at the surface of electrode. Therefore, the CNTs-COOH/GC electrode was immersed in 0.2 M Na_2SO_4 solution containing 1 mM $HAuCl_4$ and 1 mM H_2PtCl_6 solution for potentiostatic electrodeposition at a potential of -0.2 V for 400 s. During this process, adsorbed $PtCl_6^{2-}$ and $AuCl_4^-$ at the surface of CNTs-COOH film were changed into Au-PtNPs (the electrode denoted Au-PtNPs/CNTs-COOH/GC) as displayed in Fig. 1. For comparison, AuNPs/CNTs-COOH/GC electrode was also constructed by immersing the CNTs-COOH/GC modified electrode in the solution containing 1 mM $HAuCl_4$ and 0.2 M Na_2SO_4 and the constant potential of -0.2 V for 400 s was applied. Afterward, the electrode was thoroughly rinsed with water and kept at room temperature for further use. For ACF immobilization, the Au-PtNPs/CNTs-COOH/GC modified electrode was immersed in the solution containing 10 mM EDC for 1 h. The EDC-attached electrode was washed and subsequently incubated in a 3.5 µM ACF solution for 2 h at room temperature. In this process the ACF was immobilized on the modified electrode through the covalent amide bonds formed by carboxyl groups on the CNTs-COOH and the amino groups on the ACF (the electrode denoted ACF/Au-PtNPs/CNTs-COOH/GC).

In order to immobilize the BPA-aptamer, ACF/PtNPs/CNTs-COOH/GC modified electrode was dipped in the solution containing 10 mM EDC and NHS for 1h. Then, 10 µL of 5 µM BPA-aptamer was dropped at the surface of the modified electrode and left for 10 h at 4ºC. In this process, the probe oligonucleotides were immobilized on the ACF/Au-PtNPs/CNTs-COOH electrode through the formation of phosphoramidate bonds between the amino group of the ACF and phosphate group of the aptamer at 5'end [40, 41]. The detection and quantitation of BPA was performed by incubating the sensing surface in the 10 mL solution containing different concentrations of BPA for 40 min.

3. Results and discussion

3.1. Characterization of the modified *electrode by SEM*

The SEM images of the bare GC (A), CNTs-COOH/GC (B), Au-PtNPs/CNTs-COOH/GC (C) and aptamer/ACF/Au-PtNPs/CNTs-COOH/GC (D) modified electrodes are shown in Fig.2. As can be seen from Fig. 2B carbon nanotubes interlaced at the surface of

GC electrode. From Fig. 2C, a number of bright dots, namely Au and Pt nanoparticles obviously observed, suggesting the successful fabrication of Au-PtNPs on the surface of CNTs-COOH, which agree with the results published in the literature [39]. Au and PtNPs with average diameter of 37 nm and spherical form dispersedly produced at the surface of sensing interface. There would be an effective interaction between other modified materials and nanoparticles due to small size of Au-PtNPs on the side walls of CNTs-COOH. As illustrated in Fig. 2D, the morphology of the electrode surface was obviously changed by the phosphoramidate bond formation between the amino group on the film and the phosphate group of the aptamer at 5'end, which confirmed the attachment of the aptamer on to the modified electrode surface. Results mentioned above successfully demonstrated the constructing process of the modified electrode.

The elemental compositions of the aptamer/ACF/Au-PtNPs/CNTs-COOH/GC electrode were determined by EDS measurement (Fig. 3A). The peaks corresponding to Au, Pt, C, and N elements were observed, indicating the presence of Au, Pt, CNT-COOH, and aptamer at the surface of modified electrode. To further confirm the successful construction of modified electrode, WDX analysis for Au, Pt, C, and N were taken and their distributions were shown in Fig. 3B- 3E, respectively.

3.2. Optimization of measurement conditions

To obtain the best conditions in the performance of the aptamer/ACF/Au-PtNPs/CNTs-COOH/GC, some effective parameters such as aptamer concentration and the incubation time for the interaction of BPA and the surface-bound aptamer probe were optimized. The concentration of aptamer has great effects on sensitivity of aptasensor. Therefore, different concentrations of aptamer solution (0.5, 2.0, 5.0, 7.0 and 10.0 µM) were used to optimize the aptasensor concentration. Nyquist plots of EIS were recorded for different concentrations of aptamer on modified electrode. The results showed that the value of electron transfer resistance (R_{ct}) increased gradually with the increasing concentrations of aptamer solution and reached plateau regions for concentration above 5 µM, which showed the saturation of phosphoramidate bonds between ACF and aptamer.

Furthermore, BPA incubation time plays an important role on the performance and efficiency of mentioned aptasensor. In order to optimize BPA incubation time, the R_{ct} value of aptasensor after being incubated in the constant amount of BPA was recorded every 5 min for 120 min in 0.1 M PBS containing 5.0 mM $[Fe(CN)_6]^{3-/4-}$. The results revealed the linear dependence between the incubation time of BPA and R_{ct} response of modified electrode. The R_{ct} value increased by increasing the incubation time up to 40 min and then began to level

off. Based on our results, 40 min was chosen as the optimum incubation time which confirmed our previous work [32].

3.3. Electrochemical behavior of aptamer/ACF/Au-PtNPs/CNTs-COOH/GC electrode

The immobilization of each functionalized layer on GC electrode surface was confirmed through CV measurements. CVs of different modified electrodes in 0.1 M PBS containing 5.0 mM $[Fe(CN)_6]^{3-/4-}$ were shown in Fig. 4A. The bare GC electrode had obvious redox peak (curve a). The CNTs-COOH/GC (curve b) exhibited larger current response than that of bare GC electrode, which ascribed to the fact that CNTs-COOH/GC could significantly enhance the conductivity of the electrode, facilitating the electron transfer. After modification of CNTs-COOH/GC electrode with Au-PtNPs (curve c), the peak current further increased, demonstrating that these kinds of nanocomposite materials could generate synergy on electrochemical properties. When the BPA-aptamer was attached at the surface of electrode, a decreased redox peak current (curve d) was obtained. This result can be associated with the repulsion between $[Fe(CN)_6]^{3-/4-}$ redox probe molecule and negative surface charges of aptamer. By interaction of aptamer with BPA, the current signal of $[Fe(CN)_6]^{3-/4-}$ further decreased (curve e), demonstrating the conformational change of aptamer. The coverage of aptamer-BPA complex at the surface of modified electrode minimized the exposed surface area of the modified electrode, which led to retarding the interfacial electron transfer of the probe and decreasing the redox current of the marker.

EIS is an effective method to further characterize the electron transfer properties of the different modified electrodes. The measurements are generally performed in Faradaic mode, using redox-probe ferrocyanide/ferricyanide in order to focus on the variations of the R_{ct} between the solution and the electrode surface. The impedance spectra include a semicircle portion and a linear portion. The semicircle section at higher frequencies is ascribed with the electron transfer limited-process, and the linear part at lower frequencies is related to the diffusion-limited process. The interfacial resistance (R_{ct}) variations lead to the semicircle diameter changes due to the electron transferring changes from the surface of the modified electrode to $[Fe(CN)_6]^{3-/4-}$ solution. To obtain the detailed information of the EIS, a simple Randles equivalent circuit model was used to fit the experimental data. The fitting parameters involved the resistance of the solution (R_s), charge transfer resistance (R_{ct}) and Warburg impedance (Z_W) attributed to the contribution of diffusion, respectively. The R_{ct} value can be estimated from the diameter of the semicircular portion of the EIS responses. As can be observed from Fig. 4B, the R_{ct} value of the CNTs-COOH modified GC electrode (curve b) was decreased compared with the bare electrode (curve a), indicating that CNTs-

COOH can accelerate the electron transfer. After the deposition of the Au-PtNPs, the charge transfer resistance was further decreased (curve c), implying that Au-PtNPs can promote electron transfer and increase the electrode surface area. When aptamer was cast at the surface of ACF/Au-PtNPs/CNTs-COOH electrode, the value of R_{ct} was increased, which can be attributed to repulsion between the net negative charge of aptamer and the $[Fe(CN)_6]^{3-/4-}$ anions (curve d). By incubating the modified electrode in the solution containing BPA, further increase in R_{ct} value was recorded, indicating that electron transfer became more difficult (curve e). Results of EIS were agreed with those of the CVs. All those results prove that aptamer/ACF/Au-PtNPs/CNTs-COOH nanocomposite not only offers a biocompatible surface for biomolecules loading, but also provides a sensitive electric interface for further sensing.

In order to make a comparison between the applicability and efficiency of different modified electrode toward BPA determination, the DPV responses of GC electrode modified with different nanomaterials including (A) aptamer/ACF/CNTs-COOH, (B) aptamer/ACF/AuNPs/CNTs-COOH, and (C) aptamer/ACF/Au-PtNPs/CNTs-COOH before (curve a) and after (curve b) BPA capture were recorded in 0.1M PBS. As can be seen from Fig. 5, after interaction of these three electrodes with BPA, the value of current response decreased and the largest decreased current signal (ΔI) was observed for aptamer/ACF/Au-PtNPs/CNTs-COOH electrode. These results proved that all the three kinds of modified electrodes could be applied as a sensor for BPA determination and aptamer/ACF/Au-PtNPs/CNTs-COOH electrode was the most sensitive platform for BPA detection. In fact, Au-PtNPs greatly enhanced the specific surface area of CNTs-COOH/GC, resulting increased loading amount of aptamer and BPA. Therefore, aptamer/ACF/Au-PtNPs/CNTs-COOH was chosen for the subsequent experiments.

Fig. 6A exhibits the dependence of CVs of ACF/Au-PtNPs/CNTs-COOH electrode on the scan rate. It was found that the redox peak currents increased linearly with increasing scan rate in the range from 10 to 125 mV s^{-1} (Fig. 7B), demonstrating an adsorption-controlled process of ACF on Au-PtNPs/CNTs-COOH and a surface-type behavior [42]. Furthermore, the peak-to-peak potential separation was approximately 90 mV for sweep rates below 100 mV s^{-1}, reflecting facile charge transfer kinetics over this range of sweep rate. At sweep rates above 150 mV s^{-1} peak separations began to increase, indicating the charge transfer kinetics limitation.

Fig. 7 shows CVs of ACF at the surface of different modified electrodes in 0.1 M PBS solution at a scan rate of 50 mV s^{-1}. As can be seen, pairs of ill redox peaks were observed when ACF was placed at the surface of GC electrode (curve a).When ACF was cast on CNTs-

COOH/GC electrode, the peak current corresponding to ACF increased (curve b), revealing the role of CNTs-COOH as the underlying film. In order to enhance the surface area of the CNTs-COOH/GC electrode and its sensitivity for monitoring the analyte, improvement of the mentioned electrode with other nanoparticle with different properties (Au and AuPtNPs) were also performed. As illustrated, the peak currents of ACF/AuNPs/CNTs-COOH /GC (curve c), and ACF/Au-PtNPs/CNTs-COOH /GC (curve d) increased compared with the ACF/CNT-COOH/GC electrode.

The reproducibility of the aptasensor was examined by recording the current responses of five independently aptasensors in the solution containing 20 nM of BPA. According to the results, acceptable and reproducible signal with relative standard deviations (RSD) of 2.3% was obtained. Also the repeatability of proposed aptasensore was evaluated by recording six repetitive current signal of modified electrode. Based on the results, the admissible repeatability with 3.4% RSD was calculated. Moreover, the stability of the mentioned aptasensor was assessed by monitoring the peak current of ACF at the surface of modified electrode repeatedly. It was found that after 100-times test, the peak current deviated from its original response only 3.9%. Long-term stability of modified electrode was also examined by probing the current response of proposed electrode after it had been kept at 4 ºC for 8 days. No obvious changes were found during the first 6 days and the response changed less than 2.1% of the initial current response. After storing for 12 days, 14 days and 16 days, we observed that current DPV intensity maintained 94.2%, 92.7%, and 91.0% of the initial values, demonstrating the promising stability of modified electrode.

3.4 Calibration curves

Under the optimal experimental conditions, the prepared aptasensor was incubated with various concentrations of BPA and the DPV responses of modified electrode for the different concentrations of BPA was recorded. All data was replicated three times and the calibration curve was drawn based on the average of three independent measurements. The points of the calibration curve represent the average of three independent signals with RSD which are shown as error bars. As can be seen from Fig. 8, the DPV oxidation peak current of ACF in 0.1 M PBS after incubation in the solution containing BPA decreased with the concentration of BPA increasing. This means that the aptamer was folded and formation of BPA-aptamer complexes on the sensing interface caused inhibition of electron transfer of ACF. Sensitive quantitative detection of BPA was carried out by monitoring the decrease of DPV responses of ACF peak current by increasing the BPA concentration. Two calibration curves were obtained at concentration ranges of 0.1-1.0 pM and 10-700 pM. The limit of

detection (LOD) of this method was calculated ($3S_b/b$, where S_b is the standard deviation of the blanks, and b is the slope of the calibration graph) to be 0.035 pM. To further clarify the amplification of the proposed aptasensor toward BPA detection, the response characteristics of the developed aptasensor was compared to those of other BPA sensor and the results presented in Table 1. As can be seen, the analytical parameters are comparable or better than the results reported for BPA determination at the surface of other modified electrodes [43-52].

In fact, utilizing the ACF as linker and electroactive redox probe simultaneously at the surface of modified electrode can be considered as considerable novelty of present work compared with our previous reported paper [39]. The high sensitivity and selectivity of the presented strategy relies upon these amplification features: (a) the presence of the ACF molecules which immobilized on the high number of reactive carboxyl groups in CNTs-COOH through amide groups can provide a high density of aptamer on the electrode surface; (b) covalent attachment of the BPA specific aptamer to the surface of the modified electrode has been performed via phosphoramidate coupling between the amino group of ACF and phosphate group of the aptamer at 5'end; (c) the way of signal transduction in which signal produces by ACF redox indicator may greatly contribute to the observed high sensitivity, since in this way any perturbation on the electrode surface can lead to a large charge in the electron transfer characteristics of redox indicator; (d) the deposition of neatly arranged Au-PtNPs enhanced active surface area and improved the electrochemical signal.

3.5 Selectivity of aptasensor

In order to provide the convincing evidence for specific interaction of BPA and aptamer, the degree of reaction with other compound for proposed aptasensor was explored under identical experimental conditions. The assessment of the selectivity of the developed aptasensor was evaluated by choosing three phenolic compounds. Fig. 9 shows the DPV response of aptasensor in the absence (curve a) and presence (curve b) of BPA (A), hydroquinone (B), phenol (C) and 4-nitrophenol (D). It was obviously observed that a significant decrease of the DPV signals was obtained by adding 20 pM of BPA, whereas the incubation of the aptasensor with other interferences with a concentration of 1000 higher than that of BPA concentration (20 nM) showed no detectable change of DPV signals, indicating that developed aptasensor was highly specific toward BPA against other members in narcotic family. In order to further prove the specificity of our sequence toward BPA detection, the dopamine-aptamer with approximately equal size (58 bases) but different sequence was used for BPA detection (Fig. 9E).

Based on the results, no significant signal variation for BPA determination was detected in the cases of dopamine-aptamer usage; whereas when BPA-aptamer was employed the detectable signal change was recorded. These results revealed that the BPA-aptamer had high specificity and good selectivity for the discrimination of BPA compared with other sequence.

3.6 Real sample analysis

In order to demonstrate the practicality of this sensor, the recovery test was carried out by using the standard addition method. Three water samples were analyzed using three independently prepared electrodes. These samples spiked with three different concentrations of 20.0, 40.0, and 60.0 pM. BPA was determined with three replicates and the detection value was the average of three results. The recovery results of BPA in the three different matrixes were summarized in Table 2. Also, the applicability of proposed sensor in real sample analysis was further evaluated by using plastic baby bottles. For this goal, three plastic baby bottles (volume = 250 mL) were employed to test for BPA leaching. Water samples were obtained by adding 100 mL of 100 °C water into the bottles and shaking for 60 min. These water samples were analyzed with constructed aptasensor and the recoveries between 94.5 % and 103.6 % with the relative standard deviations of 2.4 % to 1.9 % were obtained, indicating that the aptasensor had good accuracy for practical application of BPA analysis in real samples.

4. Conclusion

In this work, a novel nanocomposite containing acid-oxidized carbon nanotubes (CNTs-COOH) and gold–platinum nanoparticles (Au–PtNPs) were utilized as a promising transduction platform to fabrication a highly sensitive BPA-aptasensor. Au–PtNPs, ACF and BPA-aptamer were immobilized on the surface of electrode through the electrodeposition, covalent amide and phosphoramidate bonds formation, respectively. The combination of simple way for fabricates high density Au-PtNPs nanocomposites and presence the NH_2 groups in ACF makes this platform as significant transduction to fabricate BPA-sensor. The superior electron transfer of ACF and densely populated aptamers at the surface of electrode caused lower detection limit and wider linear range for developed aptasensor. The biosensing was established by folding aptamer into the BPA-binding three-way junction upon increasing BPA and inhibition the electron transfer; consequently, the current decreased in the presence the BPA.

References

[1] R. Y. Shen, W. M. Zhang, Y. Yuan, G. Y. He, H. Q. Chen, Electrochemical detection of bisphenol A at graphene/melamine nanoparticle-modified glassy carbon electrode, J. Appl. Electrochem.45 (2015) 343–352.

[2] W. Wang, X. Yang, Y. X. Gu, C. F. Ding, J. Wan, Preparation and properties of bisphenol A sensor based on multiwalled carbon nanotubes/$Li_4Ti_5O_{12}$-modified electrode, Ionics 21 (2015) 885–893.

[3] X. Zhang, L. Wu, J. W. Zhou, X. H. Zhang, J. H. Chen, A new ratiometric electrochemical sensor for sensitive detection of bisphenol A based on poly-*β*-cyclodextrin/electroreduced graphene modified glassy carbon electrode, J. Electroanal. Chem.742 (2015) 97–103.

[4] Y. Q. Huang, C. K. Wong, J. S. Zheng, H. Bouwman, R. Barra, B. Wahlstrom, L. Neretin, M. H. Wong, Bisphenol A (BPA) in China: A review of sources, environmental levels, and potential human health impacts, Environ. Int. 42 (2012) 91–99.

[5] L. Yu, C. P. Wang, X. H. Ren, H. W. Sun, Catalytic oxidative degradation of bisphenol A using an ultrasonic-assisted tourmaline-based system: Influence factors and mechanism study, Chem. Eng. J. 252 (2014) 346–354.

[6] E. Chung, J. Jeon, J. Yu, C. Lee, J. Choo, Surface-enhanced Raman scattering aptasensor for ultrasensitive trace, Biosens. Bioelectron. 64 (2015)560–565.

[7] H. Segner, K. Caroll, M. Fenske, C. R. Janssen, G. Maack, D. Pascoe, C. Schafers, G. F. Vandenbergh, M. Watts, Identification of endocrine-disrupting effects in aquatic vertebrates and invertebrates: report from the European IDEA project, Ecotoxicol. Environ. Saf. 54 (2003) 302–314.

[8] X. Wang, X. B. Lu, L. D. Wu, J. P. Chen, 3D metal-organic framework as highly efficient biosensing platform for ultrasensitive and rapid detection of bisphenol A, Biosens. Bioelectron. 65 (2015) 295–301.

[9] H. Gallart-Ayala, E. Moyano, M. T. Galceran, Recent advances in mass spectrometry analysis of phenolicendocrine disruptors and related compounds, Mass Spectrom. Rev. 29 (2010)776–805.

[10] H. G. Ayala, E. Moyano, M. T. Galceran, Analysis of bisphenols in soft drinks by online solid phase extraction fast liquid chromatography–tandem mass spectrometry, Anal. Chim. Acta 683 (2011) 227–233.

[11] G. Gatidou, N. S. Thomaidis, A. S. Stasinakis, T. D. Lekkas, Simultaneous determination of the endocrine disrupting compounds nonylphenol, nonylphenol ethoxylates, triclosan and bisphenol A in waste water and sewage sludge by gas chromatography-mass spectrometry, J. Chromatogr. A1138 (2007) 32–41.

[12] K. Ouchi, S. Watanabe, Measurement of bisphenol A in human urine using liquid chromatography with multi-channel coulometric electrochemical detection, J. Chromatogr. B780 (2002)365–370.

[13] Y. Wen, B. S. Zhou, Y. Xu, S. W. Jin, Y. Q. Feng, Analysis of estrogens in environmental waters using polymer monolithin-poly ether ketone tube solid-phase microextraction combined with high-performance liquid chromatography, J. Chromatogr. A 1133 (2006) 21–28.

[14] T. Cirillo, G. Latini, M. A. Castaldi, L. Dipaola, E. Fasano, F. Esposito, G. Scognamiglio, F. D. Francesco, L. Cobellis, Exposuretodi-2-ethylhexyl phthalate, di-N-butyl phthalate and bisphenol A through infant formulas, J. Agric. Food Chem. 63 (2015) 3303–3310.

[15] M. Rezaee, Y. Yamini, S. Shariati, A. Esrafili, M. Shamsipur, Dispersive liquid– liquid micro extraction combined with high-performance liquid chromatography-UV detection as a very simple, rapid and sensitive method for the determination of bisphenol A in water samples, J. Chromatogr. A1216 (2009) 1511–1514.

[16] Y. Feng, B. Ning, P. Su, H. Wang, C. Wang, F. Chen, Z. Gao, An immunoassay for bisphenol A based on direct hapten conjugation to the polystyrene surface of microtiter plates, Talanta 80(2009)803–808.

[17] H. Fukata, H. Miyagawa, N. Yamazaki, C. Mori, Comparison of elisa- and LC-MS-based methodologies for the exposure assessment of bisphenol A, Toxicol. Mech. Methods16 (2006) 427–430.

[18] Y. Lu, J. R. Peterson, J. J. Gooding, N. A. Lee, Development of sensitive direct and indirect enzyme-linked immunosorbent assays (ELISAs) for monitoring bisphenol-A in canned foods and beverages, Anal. Bioanal. Chem.403 (2012) 1607–1618.

[19] Z. Mei, H. Chu, W. Chen, F. Xue, J. Liu, H. Xu, R. Zhang, L. Zheng, Ultrasensitive one-step rapid visual detection of bisphenol A in water samples by label-free aptasensor, Biosens. Bioelectron.39 (2013) 26–30.

[20] K. V. Ragavan, L. S. Selvakumar, M. S. Thakur, Functionalized aptamers as nano-bioprobes for ultrasensitive detection of bisphenol-A, Chem. Commun.49 (2013) 5960–5962.

[21] H. Kuang, H. Yin, L. Liu, L. Xu, W. Ma, C. Xu, Asymmetric plasmonic aptasensor for sensitive detection of bisphenol A, ACS Appl. Mater. Interfaces 6 (2014)364–369.

[22] H. L. Marks, M. V. Pishko, G. W. Jackson, G. L. Cote, Rational design of a bisphenol A aptamer selective surface-enhanced raman scattering nanoprobe Anal. Chem. 86(2014)11614–11619.

[23] Y. Zhu, Y. Cai, L. Xu, L. Zheng, L. Wang, B. Qi, C. Xu, Building an Aptamer/Graphene oxide FRET biosensor for one-step detection of bisphenol A, , Appl. Mater. Interfaces 7 (2015) 7492–7496.

[24] C. Deng, J. Chen, Z. Nie, M. Wang, X. Chu, X. Chen, X. Xiao, C. Lei, S. Yao, Impedimetric aptasensor with femtomolar sensitivity based on the enlargement of surface-charged gold nanoparticles, Anal. Chem. 81 (2009) 739–745.

[25] A. Sassolas, L. J. Blum, B. D. Leca-Bouvier, Electrochemical aptasensors, Electroanalysis, 21(2009) 1237–1250.

[26] H. Fan, H. Li, Q. Wang, P. He, Y. Fang, A host–guest-recognition-based electrochemical aptasensor for thrombin detection, Biosens. Bioelectron. 35 (2012) 33–36.

[27] M. Y. Ho, N. Souza, P. Migliorato, Electrochemical aptamer-based sandwich assays for the detection of explosives, Anal. Chem. 84 (2012) 4245–4247.

[28] S. Bahrami, A. R. Abbasi, M. Roushani, Z. Derikvand, A. Azadbakht, An electrochemical dopamine aptasensor incorporating silver nanoparticle, functionalized carbon nanotubes and graphene oxide for signal amplification, Talanta, 159 (2016)307-316.

[29] A. Azadbakht, M. Roushani, A. R. Abbasi, S. Menati, Z. Derikvand, A label-free aptasensor based on polyethyleneimine wrapped carbon nanotubes in situ formed gold nanoparticles as signal probe for highly sensitive detection of dopamine, Mat. Sci. Eng. C, 68(2016)585-593.

[30] Z. M. Zhou, Z. Feng, J. Zhou, B. Y. Fang, X. X. Qi, Z. Y. Ma, B. Liu, Y. D. Zhao, X. B. Hu, Capillary electrophoresis-chemiluminescence detection for carcino-embryonic antigen based on aptamer/graphene oxide structure, Biosens. Bioelectron. 64(2015)493- 498.

[31] X. Liu, J. Ren, L. Su, X. Gao,Y. Tang, T. Ma, L. Zhu, J. Li, Novel hybrid probe based on double recognition of aptamer- molecularly imprinted polymer grafted on upconversion nanoparticles for enrofloxacin sensing, Biosens. Bioelectron. 87 (2017) 203-208.

[32] Z. Derikvandi, A. R. Abbasi, M. Roushani, Z. Derikvand, A. Azadbakht, Design of ultrasensitive bisphenol A–aptamer based on platinum nanoparticles loading to polyethyleneimine-functionalized carbon nanotubes, Anal. Biochem. 512 (2016) 47-57.

[33] M. J. Song, S. K. Lee, J. Y. Lee, J. H. Kim, D. S. Lim, Electrochemical sensor based on Au nanoparticles decorated boron-doped diamond electrode using ferrocene-tagged aptamer for proton detection, J. Electroanal. Chem. 677(2012)139–144.

[34] Y. Liu, J. Yan, M. C. Howland, T. Kwa, A. Revzin, Micropatterned aAptasensors for continuous monitoring of cytokine release from human leukocytes, Anal.Chem.83 (2011) 8286–8292.

[35] M. Vrabel, P. Horakova, H. Pivonkova, L. Kalachova, H.Cernocka, H. Cahova, R. Pohl, P. Sebest, L. Havran, M. Hocek, M. Fojta, Base-modified DNA labeled by $[Ru(bpy)_3]^{2+}$ and $[Os(bpy)_3]^{2+}$ complexes: construction by polymerase incorporation of modified nucleoside triphosphates, electrochemical and luminescent properties, and applications, Chem. Eur. J. 15(2009)1144–1154.

[36] A. Bogomolova, E. Komarova, K. Reber, T. Gerasimov, O. Yavuz, S. Bhatt, M. Aldissi, Challenges of electrochemical impedance spectroscopy in protein biosensing, Anal.Chem.81(2009) 3944–3949.

[37] M. Jo, J.Y. Ahn, J. Lee, S. Lee, S.W. Hong, J.W. Yoo, J. Kang, P. Dua, D.K. Lee, S.Hong, Development of single-stranded DNA aptamers for specific bisphenol A detection, Oligonucleotides, 21 (2011) 85–91.

[38] P. Jing, H. Yi, S. Xue, Y. Chai, R. Yuan, W. Xu, A sensitive electrochemical aptasensor based on palladium nanoparticles decorated graphene–molybdenum disulfide flower-like nanocomposites and enzymatic signal amplification, Anal. Chim. Acta, 853 (2015) 234–241.

[39] A. Azadbakht, M. Roushani, A. R. Abbasi, Z. Derikvand, Design and characterization of electrochemical dopamine–aptamer as convenient and integrated sensing platform, Anal. Biochem. 507 (2016) 47–57

[40]Y. Bo, H. Y. Yang, Y. Hu, T. M. Yao, S. S. Huang, A novel electrochemical DNA biosensor based on graphene and polyaniline nanowires, Electrochimica Acta, 56 (6) (2011)2676–2681.

[41]S. Liu, X. Xing, J. Yu, W. Lian, J. Li, M. Cui, J. Huang, A novel label-free electrochemical aptasensor based on graphene–polyaniline composite film for dopamine determination, Biosens. Bioelectron. 36(1) (2012) 186 -191.

[42] E. Laviron, The use of linear potential sweep voltammetry and of a.c. voltammetry for the study of the surface electrochemical reaction of strongly adsorbed systems and of redox modified electrodes, J. Electroanal. Chem. 100 (1979) 263.

[43] W. Zhu, X. Yue, J. Duan, Y. Zhang, W. Zhang, S. Yu, Y. Wang, D. Zhang, J. Wang, Electrochemically co-reduced 3D GO-C60 nanoassembly as an efficient nanocatalyst for electrochemical detection of bisphenol S, Electrochim. Acta, 188 (2016) 85–90

[44] L. A.Goulart, F. C. Moraes, L. H. Mascaro, Influence of the different carbon nanotubes on the development of electrochemical sensors for bisphenol A, Mat. Sci. Eng. C, 58 (2016) 768–773

[45] J. Y. Wang, Y.L. Su, B. H. Wu, S. H. Cheng, Reusable electrochemical sensor for bisphenol A based on ionic liquid functionalized conducting polymer platform, Talanta,147(2016)103–110.

[46] K. J. Huang, Y. J. Liu, Y. M. Liu, L. L. Wang, Molybdenum disulfide nanoflower-chitosan-Au nanoparticles composites based electrochemical sensing platform for bisphenol A determination, J. Hazard. Mater. 276 (2014) 207–215.

[47] F. Wang, J. Yang, K. Wu, Mesoporous silica-based electrochemical sensor for sensitive determination of environmental hormone bisphenol A, Anal. Chim. Acta, 638(2009)23–28.

[48] C. Wu, Q. Cheng, L. Li, J. Chen, K. Wu, Synergetic signal amplification of graphene-Fe_2O_3 hybrid and hexadecyltrimethyl ammonium bromide as an ultra-sensitive detection platform for bisphenol A, Electrochim. Acta, 115(2014) 434–439.

[49] C. Hou, W. X. Tang, C. Zhang, Y. F. Wang, N. N. Zhu, A novel and sensitive electrochemical sensor for bisphenol A determination based on carbon black supporting ferroferric oxide nanoparticles, Electrochim. Acta, 144 (2014) 324–331.

[50] D. Pan, Y. Gu, H. Lan, Y. Sun, H. Gao, Functional graphene-gold nano-composite fabricated electrochemical biosensor for direct and rapid detection of bisphenol A, 2015. Anal. Chim. Acta, 853, 297–302.

[51] B. K. Kim, J. Y. Kim, D. H. Kim, H. N. Choi, W. Y. Lee, Electrochemical determination of bisphenol A at carbon nanotube-doped titania-nafion composite modified electrode, Bull. Korean Chem. Soc. 34 (2013) 1065.

[52] Z. X. Zheng, Y. L. Du, Z. H. Wang, Q. L. Feng, C. M. Wang, Pt/graphene-CNTs nanocomposite based electrochemical sensors for the determination of endocrine disruptor bisphenol A in thermal printing papers, Analyst, 138 (2013) 693.

Figure caption

Fig.2 Typical SEM image of bare GC (A), CNTs-COOH/GC (B), Au-PtNPs/CNTs-COOH/GC (C), and aptamer/ACF/Au-PtNPs/CNTs-COOH/GC (D) electrodes.

Fig. 3 EDS spectrum of the aptamer/ACF/Au-PtNPs/CNTs-COOH/GC electrode (A). WDX analysis for Au (B), Pt (C), C (D), and N (E) at the surface of modified electrode.

Fig. 4 Illustration of the aptasensor fabrication and corresponding CVs (A) and Nyquist plots (B) for bare GC (curve a), CNTs-COOH/GC (curve b), Au-PtNPs/CNTs-COOH/GC (curve c), aptamer/ACF/Au-PtNPs/CNTs-COOH/GC (curve d) and BPA/aptamer/ACF/Au-PtNPs/CNTs-COOH/GC (curve e) electrodes recorded in 0.1 M PBS containing 5.0 mM $[Fe(CN)_6]^{3-/4-}$.

Fig.5 DPV responses of GC electrode modified with (A) aptamer/ACF/CNTs-COOH, (B) aptamer/ACF/AuNPs/CNTs-COOH, and (C) aptamer/ACF/Au-PtNPs/CNTs-COOH before (curve a) and after (curve b) BPA grab recorded in 0.1M PBS.

Fig.6 (A) CVs of ACF/Au-PtNPs/CNTs-COOH modified electrode in 0.1 M PBS at different scan rates: 10, 20, 30, 40, 50, 60, 70, 80, 90, 100, 125, 150, 175, and 200 mV s^{-1}. (B) Plot of peak currents vs. scan rate.

Fig.7 CVs of ACF at the surface of GC (curve a), CNTs-COOH/GC (curve b), AuNPs/CNTs-COOH /GC (curve c), and Au-PtNPs/CNTs-COOH /GC (curve d) modified electrodes in 0.1 M PBS solution at a scan rate of 50 mV s^{-1}.

Fig. 8 (A) DPV obtained for prepared aptasensor recorded in 0.1 M PBS after incubation with different concentration of BPA: 0.1, 0.5, 1.0, 10, 100, 250, 500, and 700 pM. (B) Plots of oxidation peak current of ACF vs. BPA concentrations.

Fig. 9 DPV responses of prepared aptasensor before (curve a) and after (curve b) being incubated in the solution containing (A) 20 pM BPA, (B) 20 nM hydroquinone, (C) 20 nM phenol, and (D) 20 nM 4-nitrophenol. (E) DPV responses of dopamine-aptamer before (curve a) and after (curve b) incubating in the solution containing 20 pM BPA.

Table 1

Comparison between this method and other reported techniques for detection of BPA.

Electrode	Electrochemical techniue	Detection limit	Linear range	Ref.
rGO[a]-C_{60}-GCE[b]	DPV[c]	0.50 µM	1.00 - 100 µM	[43]
MWCNTs[d]/GCE	-	0.61 µM	2.50 - 29.1 µM	[44]
PEDOT[e]/BMIMBr[f]/SPCE[g]	FIA[h]	0.02 µM	0.10 -500 µM	[45]
AuNPs-CS[i]-MoS_2/ GCE/	-	0.005 µM	0.05- 100 µM	[46]
MCM-41/CPE[j]	-	0.038 µM	0.22- 8.80 µM	[47]
Gr[k]-Fe_2O_3/GCE	DPV	0.0025 µM	0.005-1.00 µM	[48]
CB[n]/Fe_3O_4/GCE	DPV	31.0 pM	0.10 nM -50.0 µM	[49]
Gr/Au-Tyr[o]-CS/GCE	DPV	1000 pM	10.0 nM - 1.00 µM	[50]
Ti/Nf[p]/CNT/GCE	LSV[q]	0.90 nM	0.01–5.00 µM	[51]
Pt/Gr–CNTs/GCE	DPV	42.0 nM	0.06-10.0 µM	[52]
This work	DPV	0.035 pM	0.10-1.00 pM 10.0 pM- 500 µM	-

a: Reduced graphene oxide

b: Glassy carbon electrode

c: Diffrential pulse voltammetry

d: Multi wall carbon nanotube

e: poly-3,4-ethylenedioxythiophene

f: Ionic liquid 1-butyl-3- methyl imidazolium bromide

g: Screen-printed carbon electrodes

h: Flow-injection amperometry

i: Chitosan

j: Carbon paste electrode

k: Graphene

n: Carbon black

o: Tyrosinase

p: Nafion

q: Linear sweep voltammetry

Sample	Spiked concentration of BPA (pM)	Measured concentration of BPA (pM)	Recovery (%)
1	20.0	19.5 ± 0.87	97.50
2	40.0	40.2± 1.22	100.5
3	60.0	58.9± 1.53	98.10

Table 2
Determination of BPA in water samples.

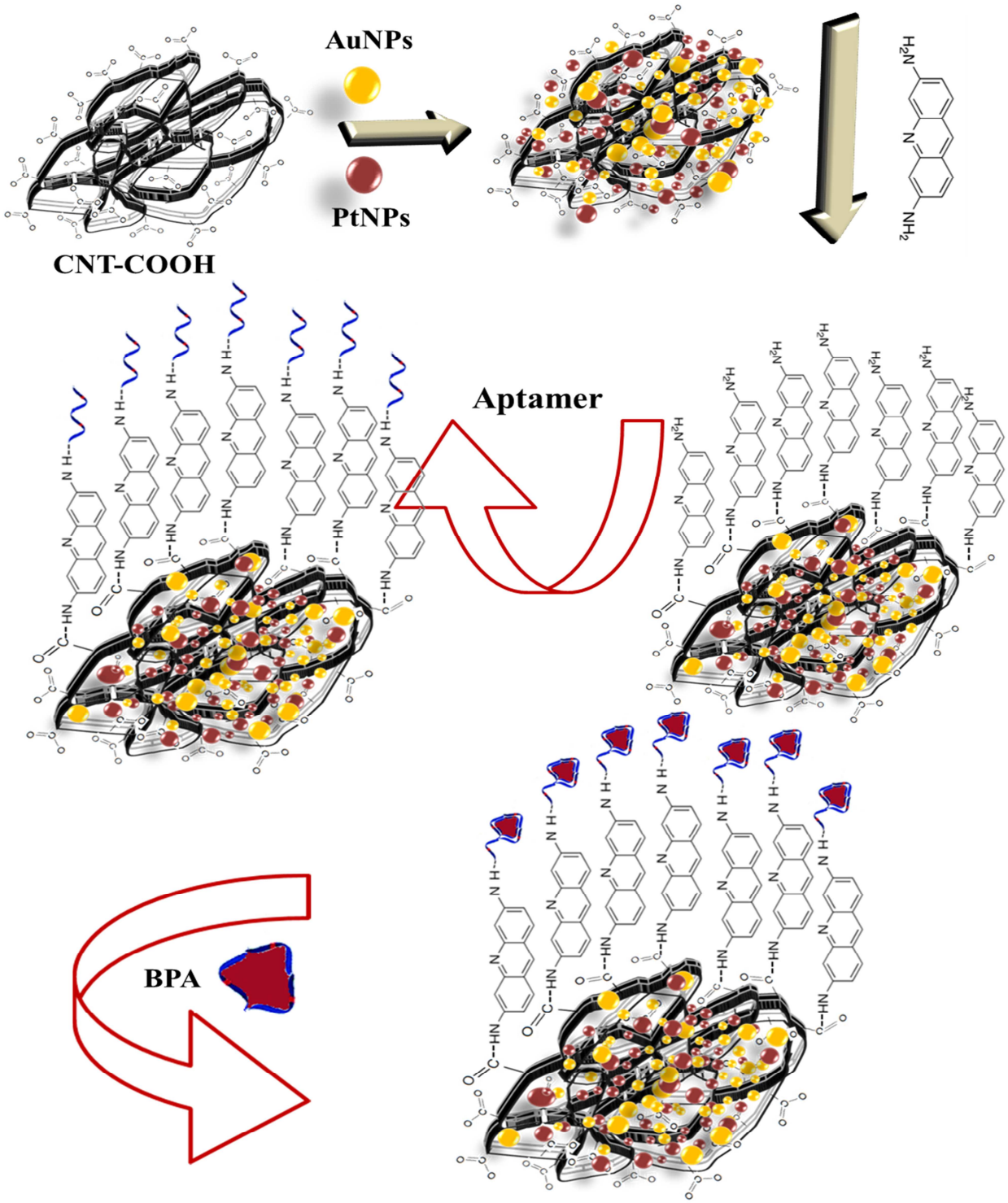

Fig.1

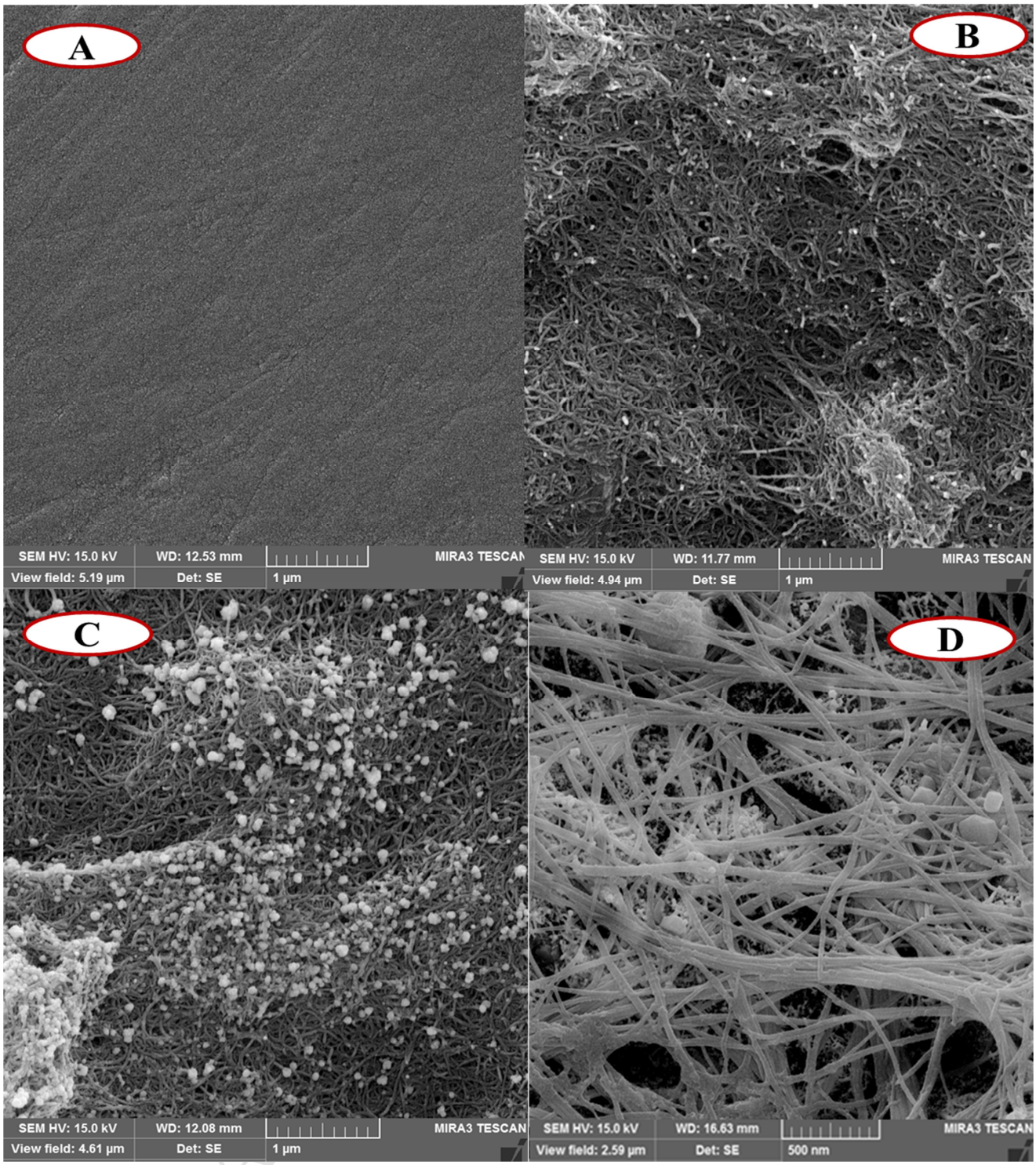
A
SEM HV: 15.0 kV
WD: 12.53 mm
MIRA3 TESCAN
View field: 5.19 µm
Det: SE
1 µm
B
SEM HV: 15.0 kV
WD: 11.77 mm
MIRA3 TESCAN
View field: 4.94 µm
Det: SE
1 µm
C
SEM HV: 15.0 kV
WD: 12.08 mm
MIRA3 TESCAN
View field: 4.61 µm
Det: SE
1 µm
D
SEM HV: 15.0 kV
WD: 16.63 mm
MIRA3 TESCAN
View field: 2.59 µm
Det: SE
500 nm

Fig.2

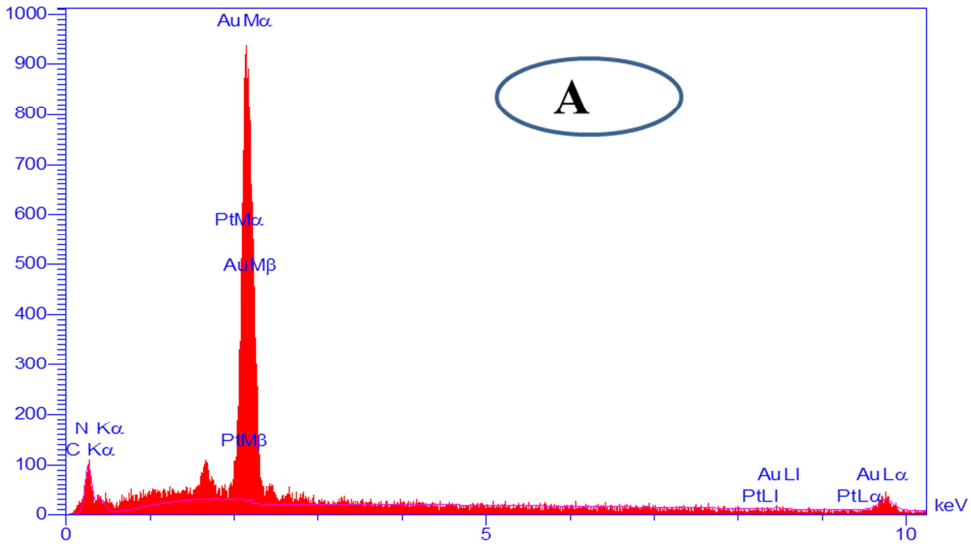
A
Au Mα
Pt Mα
Au Mβ
N Kα
C Kα
Pt Mβ
Au Ll
Pt Ll
Au Lα
Pt Lα
keV
1000
900
800
700
600
500
400
300
200
100
0
0
5
10

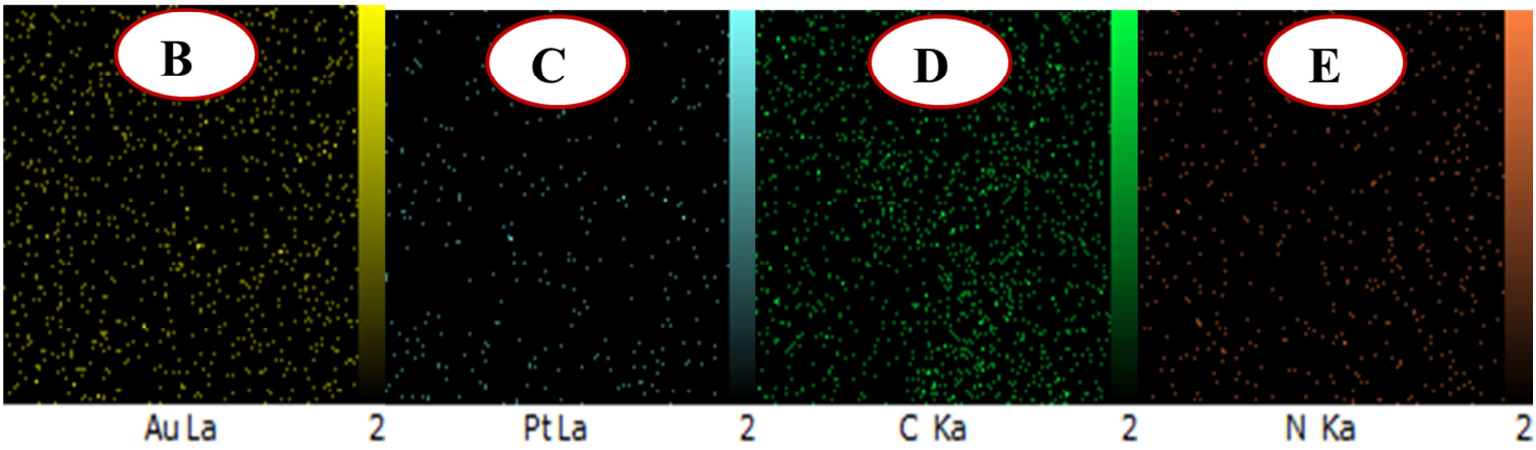
B
C
D
E
Au La
2
Pt La
2
C Ka
2
N Ka
2

Fig. 3

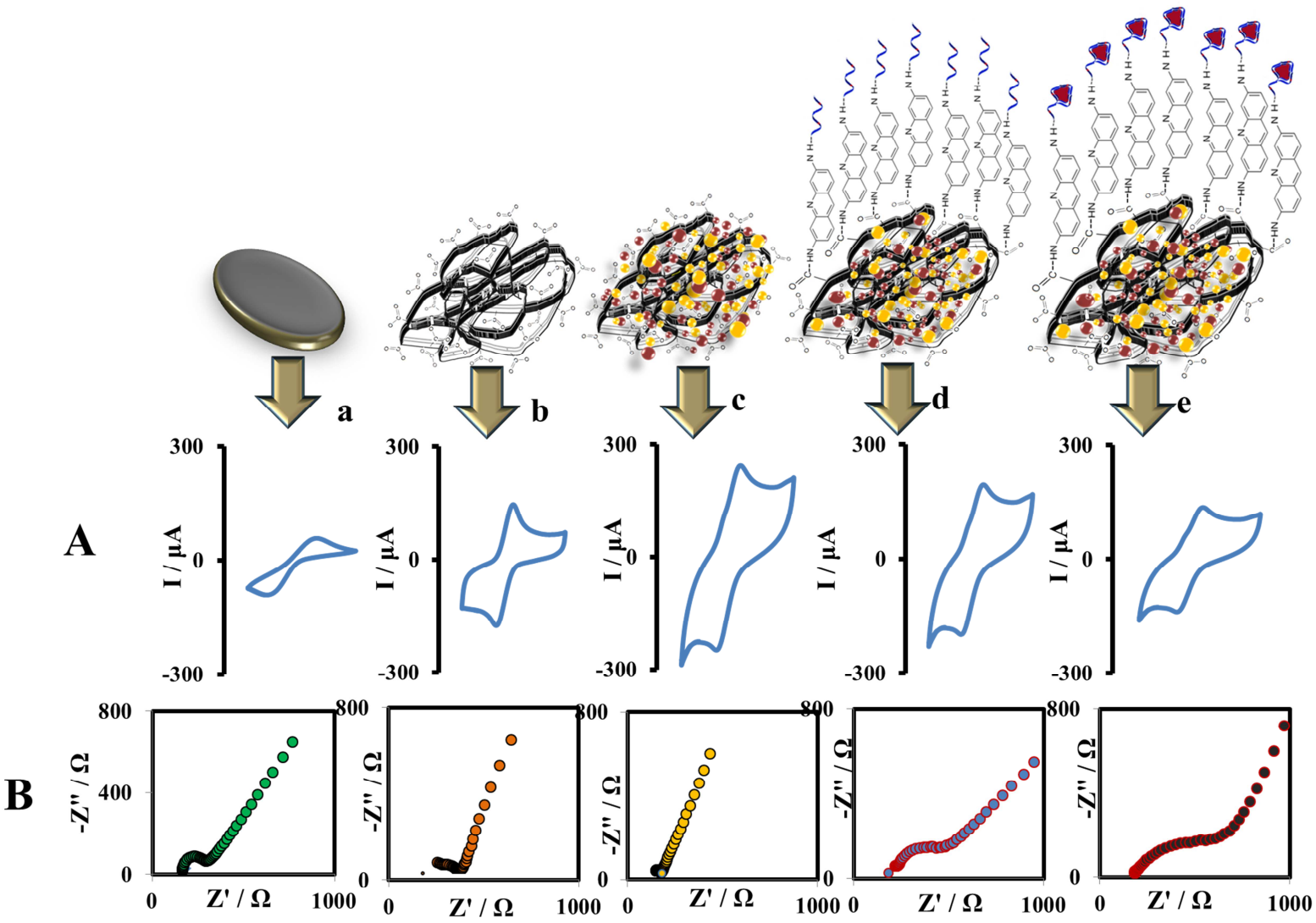

Fig. 4

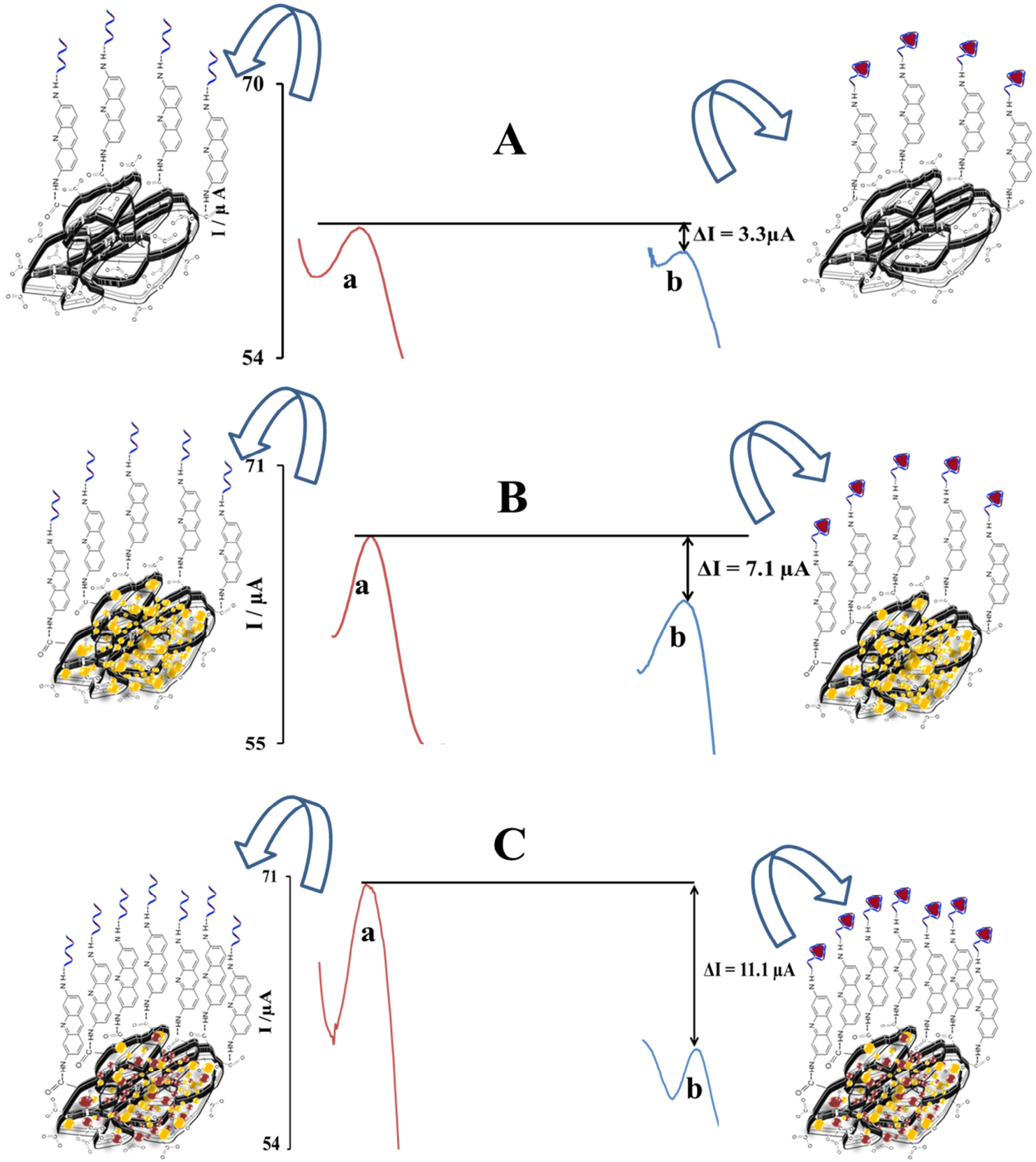

Fig. 5

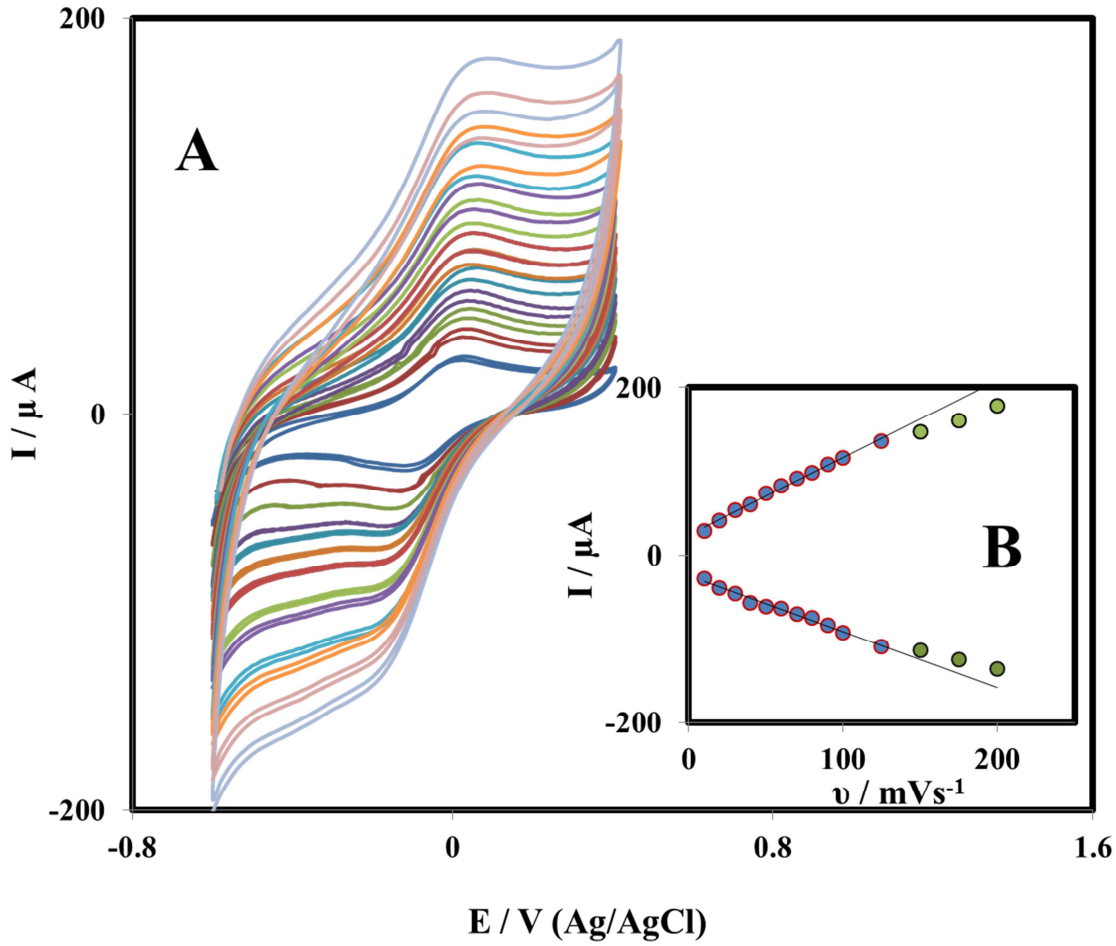

Fig. 6

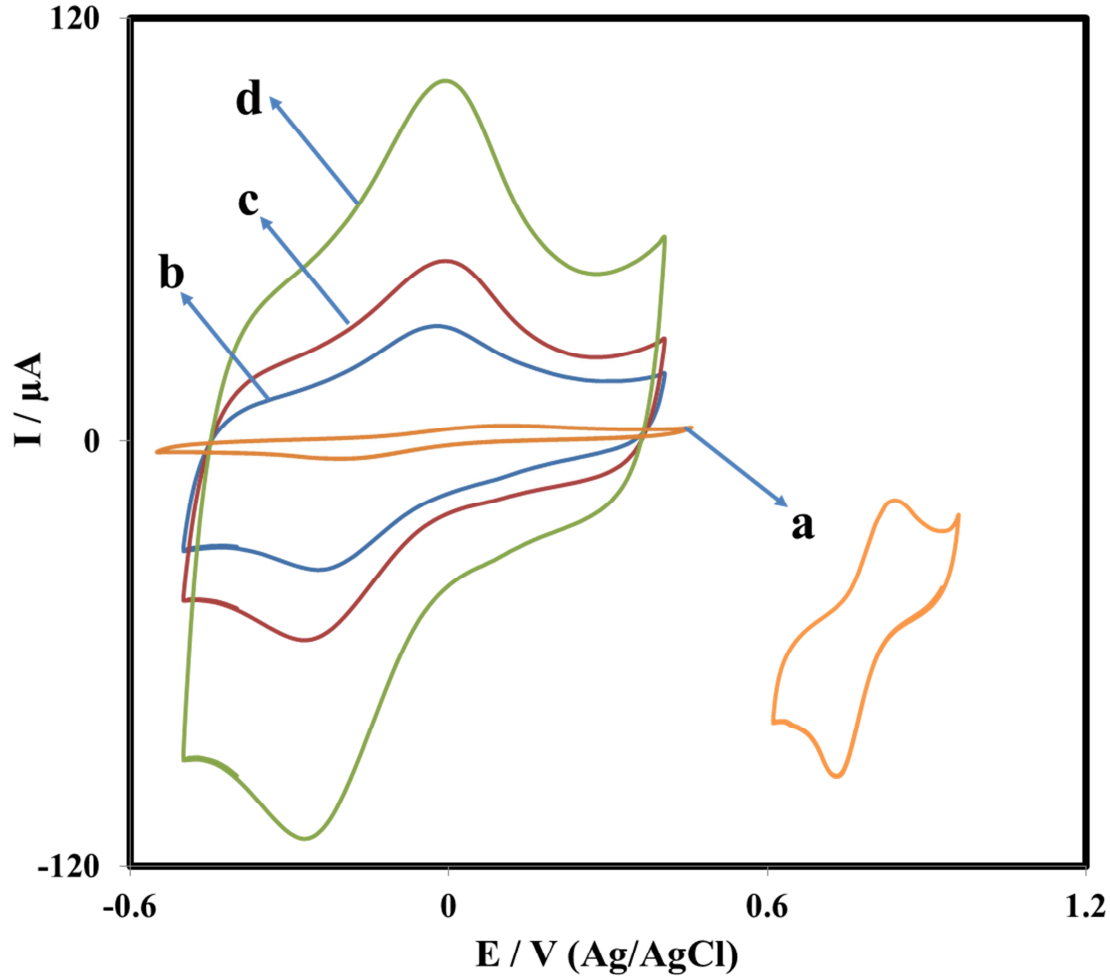

Fig. 7

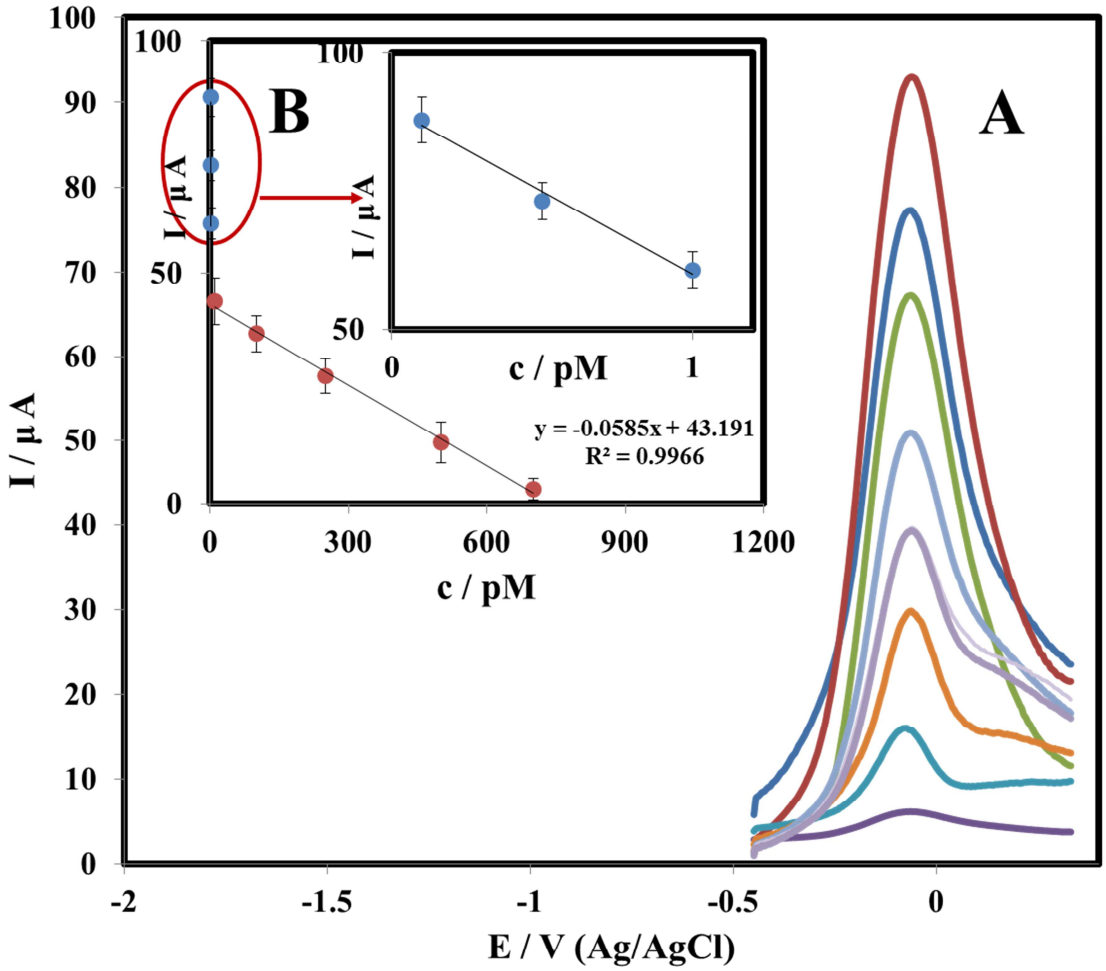

Fig. 8

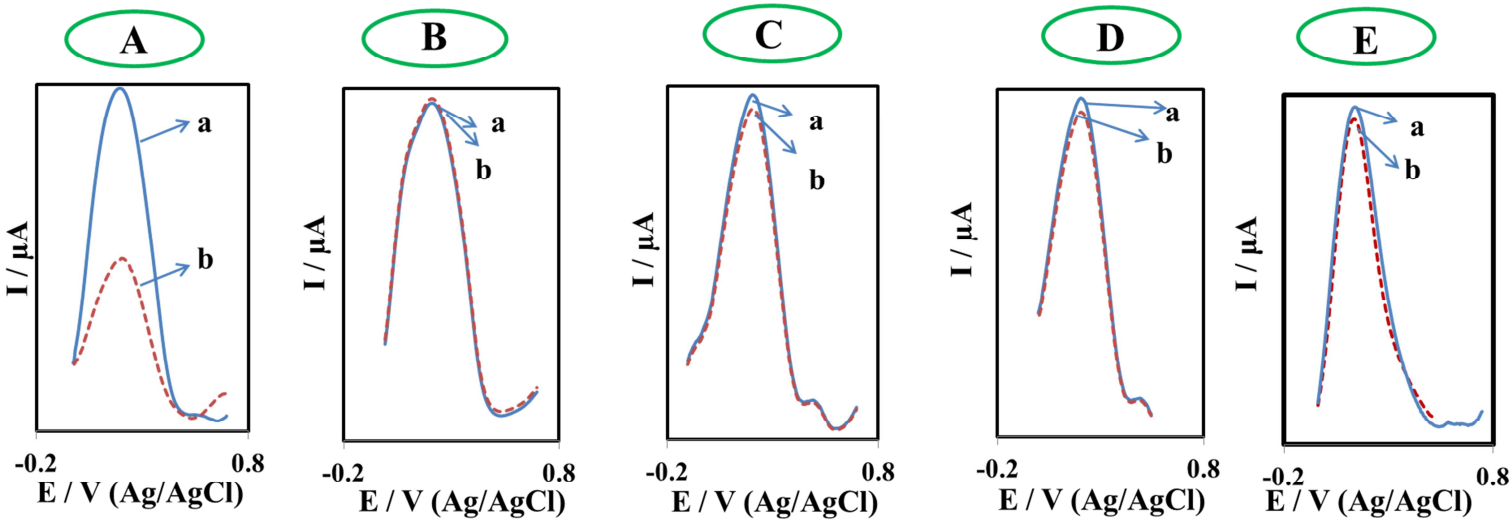

Fig. 9